# Kinetics of Iron Release from Ferric Binding Protein (FbpA): Mechanistic Implications in Bacterial Periplasm-to-Cytosol $Fe^{3+}$ Transport†

Suraj Dhungana,‡ Damon S. Anderson,§ Timothy A. Mietzner,§ and Alvin L. Crumbliss*,‡

*Department of Chemistry, Duke University, Durham, North Carolina 27708-0346, and Department of Molecular Genetics and Biochemistry, University of Pittsburgh, Pittsburgh, Pennsylvania 15261*

*Received March 24, 2005; Revised Manuscript Received April 15, 2005*

ABSTRACT: The ferric binding protein (FbpA) transports iron across the periplasmic space of certain Gram-negative bacteria and is an important component involved in iron acquisition by pathogenic *Neisseria* spp. (*Neisseria gonorrheae* and *Neisseria meningitidis*). Previous work has demonstrated that the synergistic anion, required for tight $Fe^{3+}$ sequestration by FbpA, also plays a key role in inserting $Fe^{3+}$ into the FbpA binding site. Here, we investigate the iron release process from various forms of holo-FbpA, $Fe^{3+}$-FbpA-X, during the course of a chelator competition reaction using EDTA and Tiron. $Fe^{3+}$FbpA-X represents the protein assembly complex with different synergistic anions, X = $PO_4^{3-}$ and NTA. Stepwise mechanisms of $Fe^{3+}$ release are proposed on the basis of kinetic profiles of these chelator competition reactions. $Fe^{3+}$FbpA-$PO_4$ and $Fe^{3+}$FbpA-NTA react differently with EDTA and Tiron during the $Fe^{3+}$-exchange process. EDTA replaces $PO_4^{3-}$ and NTA from the first coordination shell of $Fe^{3+}$ and acts as a synergistic anion to give a spectroscopically distinguishable intermediate, $Fe^{3+}$FbpA-EDTA, prior to pulling $Fe^{3+}$ out of the protein. Tiron, on the other hand, does not act as a synergistic anion but is a more efficient competing chelator as it removes $Fe^{3+}$ from FbpA at rate much faster than EDTA. These results reaffirm the contribution of the synergistic anion to the FbpA iron transport process as the anion, in addition to playing a facilitative role in iron binding, appears to have a "gatekeeper" role, thereby modulating the $Fe^{3+}$ release process.

Many pathogenic bacteria that cause disease in human hosts rely on iron-transport proteins as their iron source (*1*). Transferrin, the mammalian iron transport protein, is the predominant source of iron for pathogenic bacteria infecting humans. *Neisseria gonorrheae* is a Gram-negative bacterium that efficiently utilizes $Fe^{3+}$ bound to human transferrin and assimilates this element for its metabolic requirements. In contrast to many bacteria, *N. gonorrheae* foregoes the production of iron-chelating siderophores that compete for transferrin-bound iron and instead expresses surface receptors that bind transferrin directly. Iron is extracted from transferrin and transported across the outer membrane and into the periplasm by the transferrin binding protein (TbpA/TbpB) (*2*). Within the periplasm, $Fe^{3+}$ is sequestered by *f*erric *b*inding *p*rotein (FbpA)[1] which shuttles $Fe^{3+}$ across the periplasmic space where it is eventually delivered to the inner membrane transport complex composed of the FbpB permease and the FbpC ATP binding protein (*3*). Once inside the cytosol iron can be assimilated into growth essential proteins such as cytochromes (for energy generation) or ribonucleotide reductase (for DNA synthesis).

FbpA is referred to as a bacterial transferrin because of its structural and functional similarities to mammalian transferrin (*4*). FbpA and transferrin both use a similar constellation of amino acid side chains as part of the $Fe^{3+}$ binding pocket, employing two tyrosines, one carboxylic acid, and a histidine as part of the assembled coordination sphere (*5*, *6*). In addition, both require a synergistic or exogenous anion for $Fe^{3+}$ binding (*4*, *5*, *7*). FbpA is a less complex protein because it is only half the size of transferrin, is not glycosylated, and contains only a single iron binding site, thus resembling a half-transferrin.

Comparative studies between FbpA and a half-transferrin demonstrate similarities between these crucial iron transporters. One similarity is high-affinity iron binding. Both proteins bind $Fe^{3+}$ with $K_{assoc}$ values on the order of $10^{17}-10^{22}$ $M^{-1}$ (*4*, *7*, *8*) (depending on the conditions used to measure these constants), which defies the kinetics of transport, i.e., binding and release of free iron. This represents the "transferrin $Fe^{3+}$ transport dilemma". Most binding and transport proteins have affinities that range from the micromolar to nanomolar range (*9*−*21*). The unique relationship between iron transport proteins and the high affinity of these proteins for free iron suggests that transport requires an additional step for iron donation.

† A.L.C. thanks the National Science Foundation (Grants CHE 0079066 and CHE 0418006) for financial support.

* Address correspondence to this author: e-mail, alc@chem.duke.edu; phone, (919) 660-1540; fax, (919) 660-1605.

‡ Duke University.

§ University of Pittsburgh.

[1] Abbreviations: FbpA, general class of bacterial ferric binding proteins; FbpB, ferric binding protein cytoplasmic permease; FbpC, nucleotide binding protein that completes the ferric binding protein ABC transporter complex; $Fe^{3+}$FbpA-X, iron-loaded ferric binding protein with synergistic anion X; EDTA, ethylenediaminetetraacetate; NTA, nitrilotriacetate; Tiron, 4,5-dihydroxy-1,3-benezenedisulfonate; MES, 4-morpholineethanesulfonic acid; UV−vis, ultraviolet−visible.

10.1021/bi0505518 CCC: $30.25 
Published on Web 06/21/2005

In mammalian systems this transferrin $Fe^{3+}$ transport dilemma is resolved by labilization of transferrin-bound iron in part controlled by binding to the human transferrin receptor (*22*) and the acidification within the endosome (*23*). How bacteria like *N. gonorrheae* remove iron from transferrin using the transferrin receptor complex is unknown. Likewise, how iron bound to FbpA within the periplasm of the gonococcus and released to the FbpBC complex is unknown.

This study focuses on the release of iron from FbpA. FbpA uses a series of anions [e.g., phosphate, pyrophosphate, citrate, oxalate, arsenate, nitrilotriacetate (NTA)] as synergistic ligands during the iron binding process in vitro (*4*, *7*, *24*). The nature of these synergistic anions significantly influences the kinetics and thermodynamics of $Fe^{3+}$ binding: the affinity of the FbpA assembly for $Fe^{3+}$, the $Fe^{3+}/Fe^{2+}$ redox properties of $Fe^{3+}$FbpA-X, and the kinetics of proton-driven $Fe^{3+}$ release (*4*, *7*, *25*, *26*). The coordination of phosphate ester as a synergistic anion has been shown to induce ester hydrolysis, suggesting the possibility of polyphosphate hydrolysis as a parallel function of FbpA in addition to $Fe^{3+}$ transport (*27*). Facile anion exchange from $Fe^{3+}$FbpA-X has been observed (*4*, *25*, *27*), which has significant implications for the $Fe^{3+}$ chelation and release processes within the periplasmic space.

The mechanism of $Fe^{3+}$ release from $Fe^{3+}$FbpA-X is of considerable interest as the transport of the essential nutrient iron into the cytosol is directly related to bacterial virulence. An understanding of the delivery process may suggest approaches to control disease mediated by *Neisseria* spp. and other pathogens by inhibiting iron uptake. A mechanistic study of the $H^+$-driven dissociation of $Fe^{3+}$ from $Fe^{3+}$-FbpA-X suggests that the synergistic anion plays a gatekeeper role in the release process (*25*). To further explore this observation at less extreme pH conditions, we report here our investigation of competing chelator-driven dissociation of $Fe^{3+}$ from $Fe^{3+}$FbpA-X at in vivo pH (6.5). Together, these studies will allow for the development of a detailed mechanistic profile of $Fe^{3+}$ release from FbpA and further define the role of the synergistic anion.

In this work we investigate the kinetics of the $Fe^{3+}$ release process from two forms of holo-FbpA, $Fe^{3+}$FbpA-NTA and $Fe^{3+}$FbpA-$PO_4$, in an attempt to understand the mechanism of $Fe^{3+}$ release during the course of a chelator competition reaction with EDTA and Tiron. A kinetic profile of these reactions allows us to describe the effectiveness of a chelator and the role of the synergistic anion in removing $Fe^{3+}$ from $Fe^{3+}$FbpA-X. The exchange of iron from FbpA at the cytosolic membrane may take place with or without reduction to $Fe^{2+}$. Intimate knowledge of the in vitro mechanism for $Fe^{3+}$ release to compare with the reductive mechanism hypothesis (*4*) is necessary to completely evaluate the likely in vivo mechanism. Here we also compare the kinetics and mechanism of $Fe^{3+}$ release from FbpA to the well-studied chelator-facilitated $Fe^{3+}$ release from human transferrin (*28*).

## MATERIALS AND METHODS

*Reagents and Protein.* EDTA (Aldrich), Tiron (1,2-dihydroxybenzene-3,5-disulfonic acid disodium salt monohydrate; Aldrich) (Scheme 1), MES (Sigma-Aldrich), and $NaClO_4$ (Aldrich 99+%) were obtained commercially. Recombinant apo-FbpA was purified and prepared as described previously (*7*, *29*).

Scheme 1: Competing Fe(III) Chelators (A) EDTA and (B) Tiron

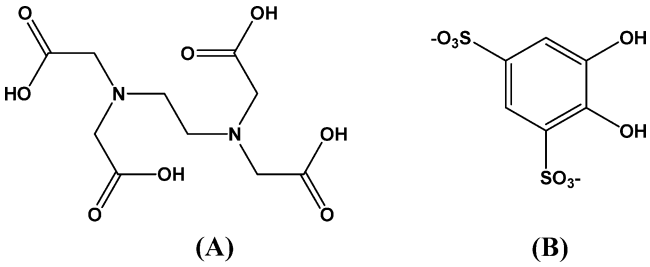


*Preparation of $Fe^{3+}$FbpA-X and Chelating Agents.* $Fe^{3+}$-FbpA-$PO_4$ and $Fe^{3+}$FbpA-NTA were prepared from apo-FbpA as described previously (*4*) and after preparation were dialyzed against 0.05 M MES buffer at pH = 6.5 with 0.1 M $NaClO_4$ as a background electrolyte. Solutions of the competing chelators, EDTA and Tiron (Scheme 1), were prepared in 0.05 M MES buffer at pH = 6.5 with 0.1 M $NaClO_4$ background electrolyte. All pH measurements were carried out using an Orion pH meter, model 230A, and the pH of the buffer solutions was adjusted with $HClO_4$ and NaOH.

*Physical Measurements.* Spectral studies were performed at 25.0 ± 0.1 °C using a Cary 100 spectrophotometer for static and slow-exchange kinetic measurements and an Applied Photophysics stopped-flow (SX.18 MV) equipped with a diode array spectrophotometer with an approximate range of 380−750 nm for rapid-exchange kinetics. Reaction kinetics were monitored in the absorbance mode, and the data were analyzed using Applied Photophysics and Sigmaplot software. The standard errors were in the range of $10^{-7}$−$10^{-8}$ when the time-dependent decay curves were fitted with single and double decay profiles. The time-resolved absorbance measurements for the competition reaction with EDTA were monitored by recording the decay in absorbance at 481 nm [$\lambda_{max}$ for the ligand to metal charge transfer (LMCT) band of $Fe^{3+}$FbpA-$PO_4$] and 467 nm ($\lambda_{max}$ for the LMCT band of $Fe^{3+}$FbpA-NTA). All exchange kinetics with Tiron were monitored by measuring the absorbance at 470 nm corresponding to the formation of the $Fe(III)(Tiron)_3^{9-}$ complex using Applied Photophysics stopped-flow (SX.18 MV) equipment. Slow kinetic experiments involving the reaction between $Fe^{3+}$FbpA-$PO_4$/$Fe^{3+}$FbpA-NTA and EDTA (stage II) were monitored using a Cary 100 spectrophotometer with rapid mixing. In these experiments reactants were mixed in a conventional spectrophotometer cuvette, and the reaction was monitored within 15 s of mixing. Each kinetic data point in the figures represents an average of three to five replicate runs.

## RESULTS

*General Considerations.* The kinetics of $Fe^{3+}$ release from two different forms of holo-FbpA, $Fe^{3+}$FbpA-$PO_4$ and $Fe^{3+}$-FbpA-NTA, were studied at pH 6.5 using two different competing chelators, EDTA and Tiron (Scheme 1). This approach allows us to study the influence of both the synergistic anion and competing chelator on the kinetics of $Fe^{3+}$ release from FbpA. In biocoordination chemistry terms, this study will determine the influence of the leaving group ($PO_4^{3-}$ or NTA) and entering group (EDTA or Tiron) on the exchange kinetics. The overall exchange reaction is

represented by the equation:

$$Fe^{3+}FbpA\text{-}X + Y \rightarrow FeY + apo\text{-}FbpA\text{-}X \qquad (1)$$

where X represents the synergistic anion required for $Fe^{3+}$ binding by FbpA ($PO_4^{3-}$ or NTA) and Y represents the competing chelator (EDTA or Tiron) used for $Fe^{3+}$ removal from $Fe^{3+}$FbpA-X. Degrees of protonation and the charges in eq 1 are omitted for clarity.

*$Fe^{3+}$FbpA-X + EDTA.* The reaction between EDTA and $Fe^{3+}$FbpA-X (X = $PO_4^{3-}$ or NTA) proceeds in two well-separated stages (stage I and stage II). The kinetic profile within stage I differs for the two forms of the protein but is the same for stage II.

At the end of stage I, both $Fe^{3+}$FbpA-$PO_4$ ($\lambda_{max}$ = 481 nm) and $Fe^{3+}$FbpA-NTA ($\lambda_{max}$ = 467 nm) exhibit a spectral shift and stabilization in $\lambda_{max}$ at ca. 460 nm. This is attributed to the formation of a quasi-equilibrium species at the end of stage I of composition $Fe^{3+}$FbpA-EDTA, with EDTA filling the role of the synergistic anion. This structural assignment is based on the spectral similarity to $Fe^{3+}$FbpA-NTA ($\lambda_{max}$ = 467 nm) where the NTA synergistic anion is structurally similar to EDTA. Furthermore, a recent crystal structure of a mutated FbpA (*mut*FbpA) shows that EDTA can act as a synergistic anion to give $Fe^{3+}$*mut*FbpA-EDTA (*30*, *31*), and similarly, the iron binding proteins serum transferrin and ovotransferrin, structurally and functionally similar to FbpA, also have been shown to use EDTA as a synergistic anion (*32*). Consequently, we propose that both $Fe^{3+}$FbpA-$PO_4$ and $Fe^{3+}$FbpA-NTA react with EDTA in stage I to form a spectroscopically identical intermediate, $Fe^{3+}$FbpA-EDTA, which appears not to include the original synergistic anion, $PO_4^{3-}$ or NTA. Residual binding of $PO_4^{3-}$ or NTA to the protein surface and not to the $Fe^{3+}$ ion may or may not occur.

The comparative crystal structure analysis of $Fe^{3+}$*mut*FbpA-EDTA and $Fe^{3+}$FbpA-$PO_4$ indicates that the $Fe^{3+}$ binding cleft for the $Fe^{3+}$*mut*FbpA-EDTA is much more exposed and accessible to solvent and other molecules (*30*, *31*). By analogy, the production of $Fe^{3+}$FbpA-EDTA as an intermediate during the kinetic experiments will conceivably generate a FbpA assembly with an exposed $Fe^{3+}$ center susceptible to attack by another EDTA molecule, facilitating $Fe^{3+}$ release. Stage II for $Fe^{3+}$FbpA-$PO_4$ and $Fe^{3+}$FbpA-NTA shows equivalent time-resolved decays in absorbance at $\lambda_{max}$ = 460 nm, which is attributed to the depletion of the intermediate $Fe^{3+}$FbpA-EDTA complex with $Fe^{3+}$ release to produce FeEDTA and apo-FbpA.

*$Fe^{3+}$FbpA-$PO_4$ + EDTA.* The stage I and stage II successive absorbance decays corresponding to the reaction between $Fe^{3+}$FbpA-$PO_4$ and EDTA (eq 1; X = $PO_4^{3-}$, Y = EDTA) both follow a single exponential profile. The time-dependent absorbance decay data recorded for each stage were fitted using the equation:

$$Abs_t - Abs_{eq} = Be^{-k_{obs}t} \qquad (2)$$

where $Abs_t$ is the time-dependent absorbance, $Abs_{eq}$ is the absorbance at the equilibrium position, $k_{obs}$ is the rate constant associated with the decay profile, and *B* is the decay amplitude.

*(A) Stage I for $Fe^{3+}$FbpA-$PO_4$ + EDTA.* A representative time-dependent spectral change for stage I of the reaction between $Fe^{3+}$FbpA-$PO_4$ and EDTA is shown in Figure 1A. The $\lambda_{max}$ = 481 nm corresponding to $Fe^{3+}$FbpA-$PO_4$ decreases in intensity by 25−30% and shifts to 460 nm in a single exponential decay over time (Figure 1). The apparent rate constant for the decay process in stage I ($k^I_{obs}$) is dependent on the EDTA concentration and exhibits saturation at high EDTA concentration (Figure 2). These results are attributed to a two-step process consisting of a rapidly established pre-equilibrium (reaction 3) followed by a rate-determining step (reaction 4), with a rate law described by eq 5. $Fe^{3+}$FbpA-$PO_4$···EDTA represents a nonspecific interaction between $Fe^{3+}$FbpA-$PO_4$ and EDTA. A nonlinear

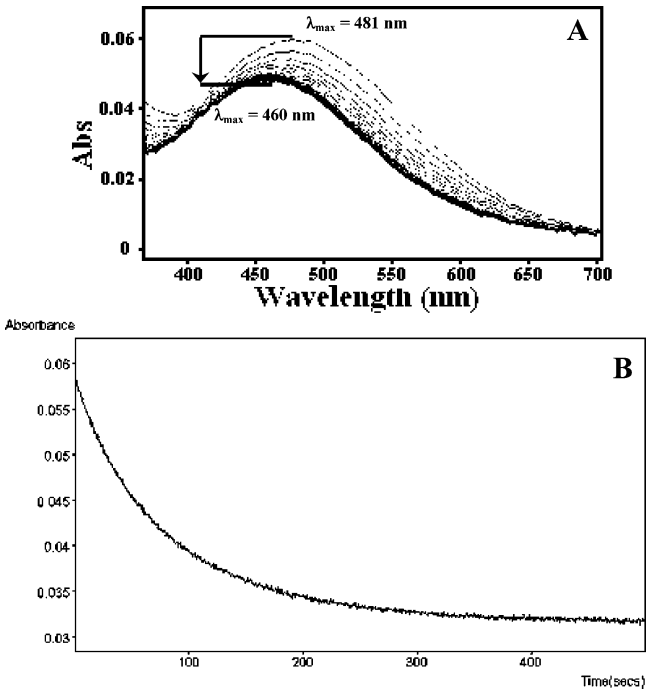


FIGURE 1: (A) Representative spectral changes corresponding to stage I of the reaction between $Fe^{3+}$FbpA-$PO_4$ and EDTA under pseudo-first-order conditions (EDTA in excess). (B) A representative absorbance decay profile at 481 nm. Data presented for (A) and (B) are from different experiments under identical conditions. Conditions for (A) and (B): [$Fe^{3+}$FbpA-$PO_4$] = $9.26 \times 10^{-5}$ M, [EDTA] = $2.5 \times 10^{-3}$ M, pH 6.5, 0.05 M MES, 0.1 M $NaClO_4$, 25 °C.

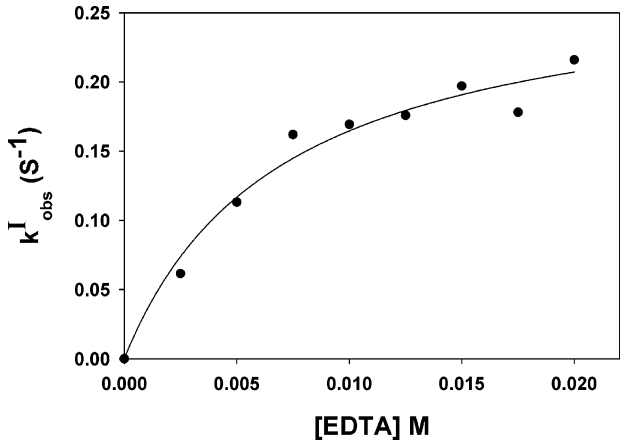


FIGURE 2: Plot of the observed stage I rate constants ($k^I_{obs}$) as a function of EDTA concentration for the reaction between $Fe^{3+}$-FbpA-$PO_4$ and EDTA. The solid line represents a nonlinear fit of eq 5 to the data. Conditions: [$Fe^{3+}$FbpA-$PO_4$] = $9.26 \times 10^{-5}$ M, pH 6.5, 0.05 M MES, 0.1 M $NaClO_4$, 25 °C.

$$Fe^{3+}FbpA\text{-}PO_4 + EDTA \rightleftharpoons Fe^{3+}FbpA\text{-}PO_4\cdots EDTA \qquad Q_1 \quad (3)$$

$$Fe^{3+}FbpA\text{-}PO_4\cdots EDTA \rightarrow Fe^{3+}FbpA\text{-}EDTA + PO_4^{3-} \qquad k_2 \quad (4)$$

$$k^{I}_{obs} = \frac{k_2[EDTA]}{(1/Q_1) + [EDTA]} \quad (5)$$

fit of eq 5 to the data (Figure 2) yields the microscopic constants, $Q_1 = 1.43 \times 10^2\ M^{-1}$ and $k_2 = 2.8 \times 10^{-1}\ s^{-1}$.

*(B) Stage II for $Fe^{3+}FbpA\text{-}PO_4$ + EDTA.* At the end of stage I the $\lambda_{max}$ has shifted and stabilized at 460 nm. Stage II shows further decrease in absorbance at 460 nm in a slow process requiring several hours for completion, which ultimately results in a complete loss in the LMCT band (due to the protein coordination to $Fe^{3+}$). The decay profile follows a single exponential (Figure 3A) according to eq 2, which is linearly dependent on the EDTA concentration (Figure 3B). A mechanism and the associated rate law consistent with these data are shown in the equations:

$$Fe^{3+}FbpA\text{-}EDTA + EDTA \rightleftharpoons apo\text{-}FbpA + FeEDTA \qquad k_3, k_{-3} \quad (6)$$

$$k^{II}_{obs} = k_3[EDTA] + k_{-3} \quad (7)$$

where $k_3$ and $k_{-3}$ represent the microscopic forward and reverse rate constants. The complete disappearance of the LMCT band in the visible spectral region supports the formation of apo-FbpA and FeEDTA. Apo-FbpA may be present as apo-FbpA-EDTA or apo-FbpA-$PO_4$. Under the given experimental conditions we cannot differentiate between possible apo-FbpA species, and more importantly they do not change our data analysis or the interpretation of the results. A linear fit of eq 7 to the data (Figure 3B) gives $k_3 = 5.7 \times 10^{-3}\ M^{-1}\ s^{-1}$ and $k_{-3} = 2.3 \times 10^{-5}\ s^{-1}$ from the slope and intercept.

*$Fe^{3+}FbpA\text{-}NTA$ + EDTA.* Similar to the reaction between $Fe^{3+}FbpA\text{-}PO_4$ and EDTA, the reaction between $Fe^{3+}FbpA$-NTA and EDTA also occurs in two stages, stage I and stage II. However, the stage I absorbance decay followed a double exponential profile according to the equation:

$$Abs_t - Abs_{eq} = Be^{-k^{I}_{1obs}t} + Ce^{-k^{I}_{2obs}t} \quad (8)$$

where $Abs_t$ and $Abs_{eq}$ are the time-dependent and equilibrium absorbance, respectively, $k^{I}_{1obs}$ and $k^{I}_{2obs}$ are two rate constants associated with the double exponential decay profile, and $B$ and $C$ are the corresponding amplitudes. The time-dependent absorbance decay corresponding to stage II showed a single-exponential profile similar to that seen for $Fe^{3+}FbpA\text{-}PO_4$, and the data were fitted using eq 2.

*(A) Stage I for $Fe^{3+}FbpA\text{-}NTA$ + EDTA.* Stage I of the reaction between $Fe^{3+}FbpA$-NTA and EDTA is distinctly different from that seen for the $Fe^{3+}FbpA\text{-}PO_4$ system. The $\lambda_{max} = 467$ nm corresponding to $Fe^{3+}FbpA$-NTA decreases with a slight blue shift to 460 nm. Representative spectral change profiles are summarized in Figure 4. The decay profile follows a double exponential (eq 8) and results in

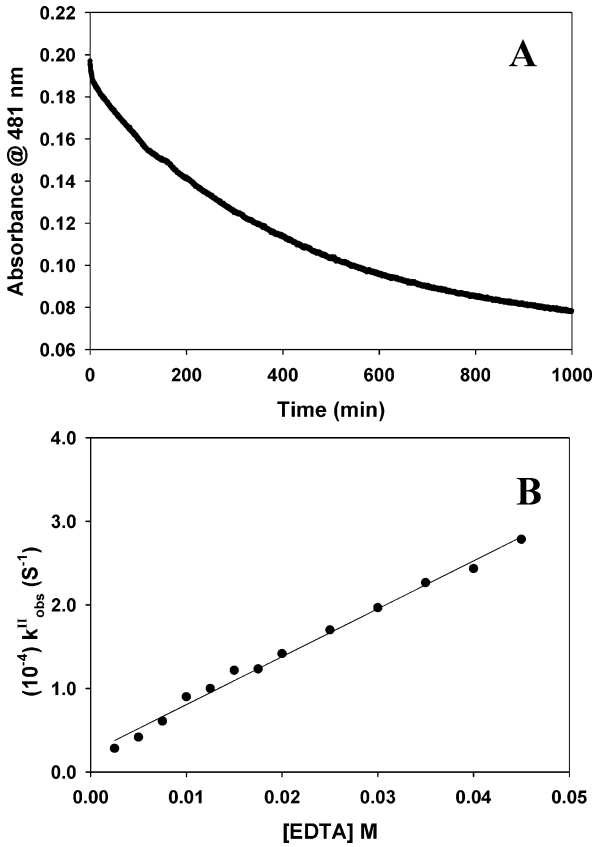


FIGURE 3: (A) A representative absorbance decay profile for stage II of the reaction between $Fe^{3+}FbpA\text{-}PO_4$ and EDTA under pseudo-first-order conditions (EDTA in excess). Conditions: $[Fe^{3+}FbpA\text{-}PO_4] = 9.26 \times 10^{-5}$ M, [EDTA] $= 2.5 \times 10^{-3}$ M, pH 6.5, 0.05 M MES, 0.1 M $NaClO_4$, 25 °C. (B) Plot of the observed stage II rate constants ($k^{II}_{obs}$) for the reaction between $Fe^{3+}FbpA\text{-}PO_4$ and EDTA. The solid line represents the linear fit of eq 7 to the data. Conditions: $[Fe^{3+}FbpA\text{-}PO_4] = 9.26 \times 10^{-5}$ M, pH 6.5, 0.05 M MES, 0.1 M $NaClO_4$, 25 °C.

~50% absorbance loss. The larger rate constant ($k^{I}_{1obs}$) shows a saturation profile at high EDTA concentrations, while the smaller rate constant ($k^{I}_{2obs}$) is linearly dependent on the EDTA concentration (Figure 5). This behavior is interpreted to be due to two competing parallel paths for the reaction between $Fe^{3+}FbpA$-NTA and EDTA. The larger rate constant is attributed to two successive reactions shown in eqs 9 and 10. Assuming reaction 9 is a rapidly established preequilibrium to the rate-determining reaction 10, the rate law may be described by eq 11:

$$Fe^{3+}FbpA\text{-}NTA + EDTA \rightleftharpoons Fe^{3+}FbpA\text{-}NTA\cdots EDTA \qquad Q_1 \quad (9)$$

$$Fe^{3+}FbpA\text{-}NTA\cdots EDTA \rightarrow Fe^{3+}FbpA\text{-}EDTA + NTA \qquad k_2 \quad (10)$$

$$k^{I}_{1obs} = \frac{k_2[EDTA]}{(1/Q_1) + [EDTA]} \quad (11)$$

where $Q_1$ represents the equilibrium constant associated with the formation of the outer-sphere assembly $Fe^{3+}FbpA$-NTA$\cdot\cdot\cdot$EDTA and $k^{I}_{1obs}$ is the apparent rate constant. A nonlinear fit of eq 11 to the data (Figure 5A) yields the microscopic

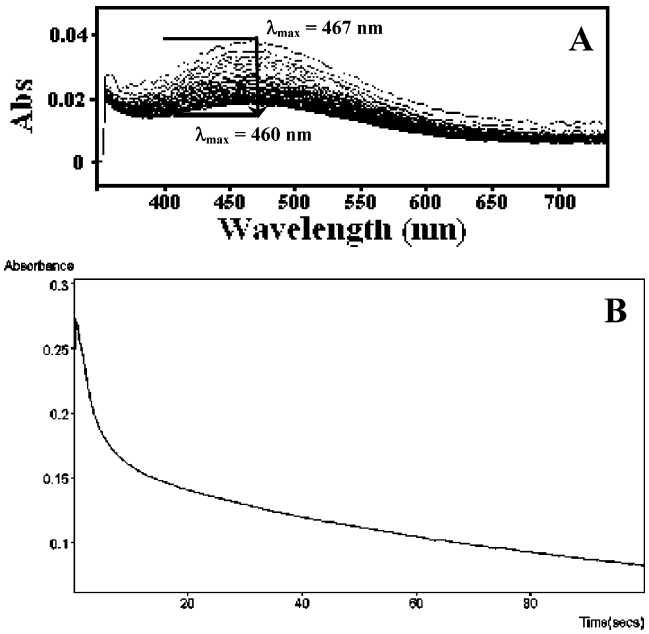


FIGURE 4: (A) Representative time-dependent spectral changes corresponding to stage I of the reaction between $Fe^{3+}$FbpA-NTA and EDTA under pseudo-first-order conditions (EDTA in excess). (B) A representative absorbance decay profile at 467 nm. Data presented for (A) and (B) are from different experiments under identical conditions. Conditions for (A) and (B): [$Fe^{3+}$FbpA-NTA] = $1.02 \times 10^{-4}$ M, [EDTA] = $5.0 \times 10^{-3}$ M, pH 6.5, 0.05 M MES, 0.1 M $NaClO_4$, 25 °C.

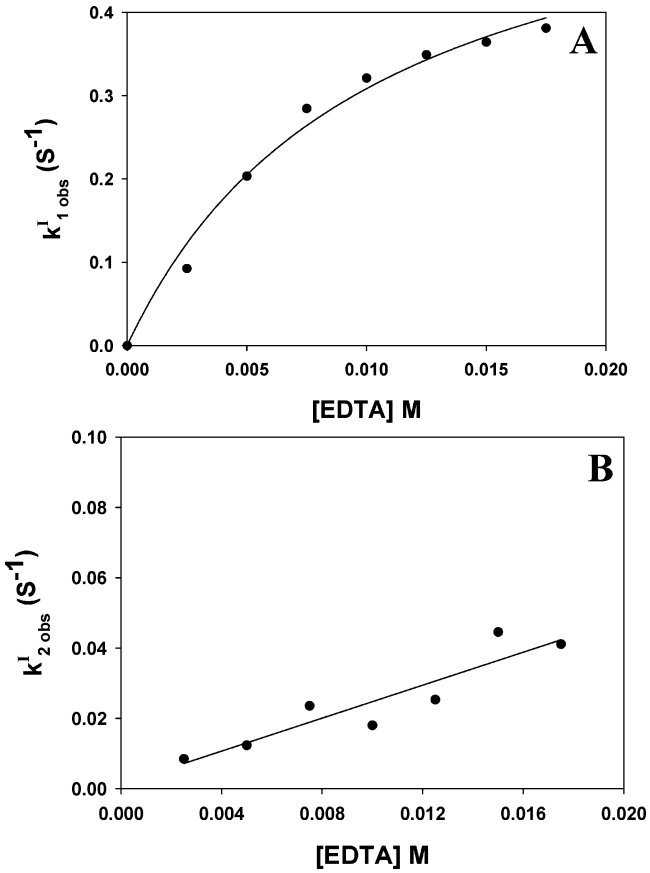


FIGURE 5: (A) Plot of the observed stage I larger rate constants ($k^I_{1obs}$) for the reaction between $Fe^{3+}$FbpA-NTA and EDTA. The solid line represents the nonlinear fit of eq 11 to the data. (B) Plot of the observed stage I smaller rate constants ($k^I_{2obs}$) for the reaction between $Fe^{3+}$FbpA-NTA and EDTA. The solid line represents the fit of eq 13 to the data. Conditions for (A) and (B): [$Fe^{3+}$FbpA-NTA] = $1.02 \times 10^{-4}$ M, pH 6.5, 0.05 M MES, 0.1 M $NaClO_4$, 25 °C.

constants, $Q_1 = 0.98 \times 10^2$ $M^{-1}$ and $k_2 = 6.2 \times 10^{-1}$ $s^{-1}$. This reaction profile is equivalent to that seen for the EDTA reaction with $Fe^{3+}$FbpA-$PO_4$, within experimental uncertainty.

The smaller rate constant ($k^I_{2obs}$) shows a linear dependency on the EDTA concentration. Such behavior is attributed to the direct attack of EDTA on $Fe^{3+}$FbpA-NTA to form an $Fe^{3+}$FbpA-EDTA intermediate complex as shown in eq 12, with the corresponding rate law in eq 13. A linear fit of eq

$$Fe^{3+}\text{FbpA-NTA} + \text{EDTA} \rightleftharpoons Fe^{3+}\text{FbpA-EDTA} + \text{NTA} \qquad k'_1, k'_{-1} \quad (12)$$

$$k^I_{2obs} = k'_1[\text{EDTA}] + k'_{-1} \quad (13)$$

13 to the data (Figure 5B) gives $k'_1 = 2.3$ $M^{-1}$ $s^{-1}$ and $k'_{-1} = 1.3 \times 10^{-3}$ $s^{-1}$ from the slope and intercept, respectively.

*(B) Stage II for $Fe^{3+}$FbpA-NTA + EDTA.* Stage II of the reaction between $Fe^{3+}$FbpA-NTA and EDTA is equivalent to stage II of the reaction between $Fe^{3+}$FbpA-$PO_4$ and EDTA described above. The slow absorbance decrease at 460 nm due to the depletion of the intermediate $Fe^{3+}$FbpA-EDTA formed at the end of stage I upon further reaction with EDTA ultimately results in a complete loss in the LMCT band corresponding to $Fe^{3+}$ binding to FbpA. The decay profile follows a single exponential (Figure 6A) and is fitted using eq 2. The apparent rate constant for the decay process ($k^{II}_{obs}$) is linearly dependent on the EDTA concentration (Figure 6B). The proposed mechanism and rate law correspond to eqs 6 and 7. A linear fit of eq 7 to the data (Figure 6B) yields $k_3 = 1.1 \times 10^{-3}$ $M^{-1}$ $s^{-1}$ and $k_{-3} = 4.2 \times 10^{-5}$ $s^{-1}$ from the slope and intercept, respectively.

*$Fe^{3+}$FbpA-X + Tiron.* Although the reactions with Tiron (Scheme 1) also occur in two stages, their profiles are distinctly different from the reactions with EDTA. This is indicative of the formation of different reaction intermediates as presented below. The changes in spectral profiles associated with the reaction between Tiron and $Fe^{3+}$FbpA-$PO_4$ and $Fe^{3+}$FbpA-NTA are similar, and representative stage I and stage II data for $Fe^{3+}$FbpA-NTA are shown in Figure 7. Initially, the $\lambda_{max}$ corresponding to the LMCT band of the $Fe^{3+}$-loaded protein undergoes a red shift (from 481 nm for $Fe^{3+}$FbpA-$PO_4$ or 467 nm for $Fe^{3+}$FbpA-NTA) to 520 nm, corresponding to stage I of the reaction. This new absorbance maximum at quasi-equilibrium then shifts to 470 nm, corresponding to the characteristic LMCT band due to the triscatecholateiron(III) complex ($Fe(Tiron)_3^{9-}$) (*33*), during stage II of the reaction. These two stages are well separated for the $Fe^{3+}$FbpA-NTA complex and display two distinct single exponential absorbance increases (Figure 7). For the $Fe^{3+}$FbpA-$PO_4$ system the two processes could not be isolated and analyzed separately but were observed and studied as a double exponential profile.

*$Fe^{3+}$FbpA-$PO_4$ + Tiron.* A time-dependent absorbance increase profile for the reaction between $Fe^{3+}$FbpA-$PO_4$ and Tiron (Figure 8) is fitted with a double exponential (eq 8), corresponding to stage I and stage II. Both rate constants

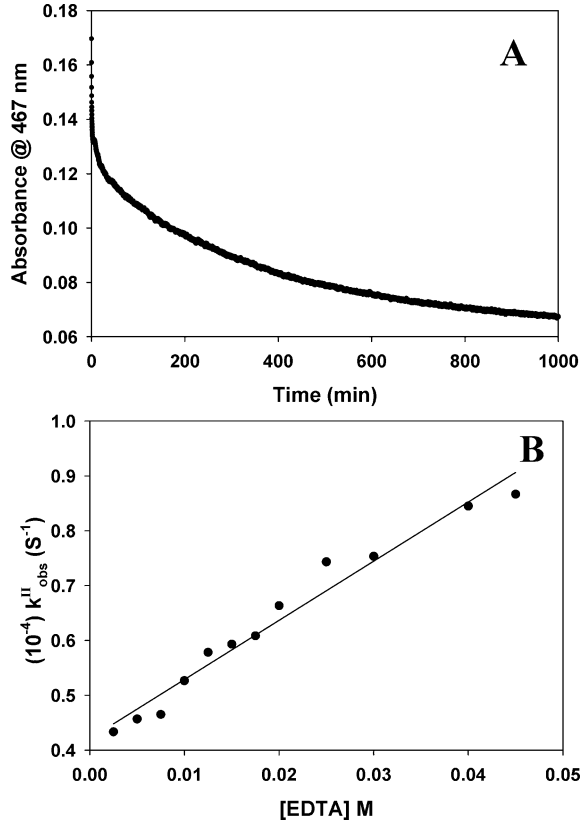


FIGURE 6: (A) A representative absorbance decay profile for stage II of the reaction between $Fe^{3+}$FbpA-NTA and EDTA under pseudo-first-order conditions (EDTA in excess). A remnant of stage I is also observed at the initial stages of the reaction. Conditions: [$Fe^{3+}$FbpA-NTA] = $1.02 \times 10^{-4}$ M, [EDTA] = $2.5 \times 10^{-3}$ M, pH 6.5, 0.05 M MES, 0.1 M $NaClO_4$, 25 °C. (B) Plot of the observed stage II rate constants ($k^{II}_{obs}$) for the reaction between $Fe^{3+}$FbpA-NTA and EDTA as a function of EDTA concentration. The solid line represents the linear fit of eq 7 to the data. Conditions: [$Fe^{3+}$FbpA-NTA] = $1.02 \times 10^{-4}$ M, pH 6.5, 0.05 M MES, 0.1 M $NaClO_4$, 25 °C.

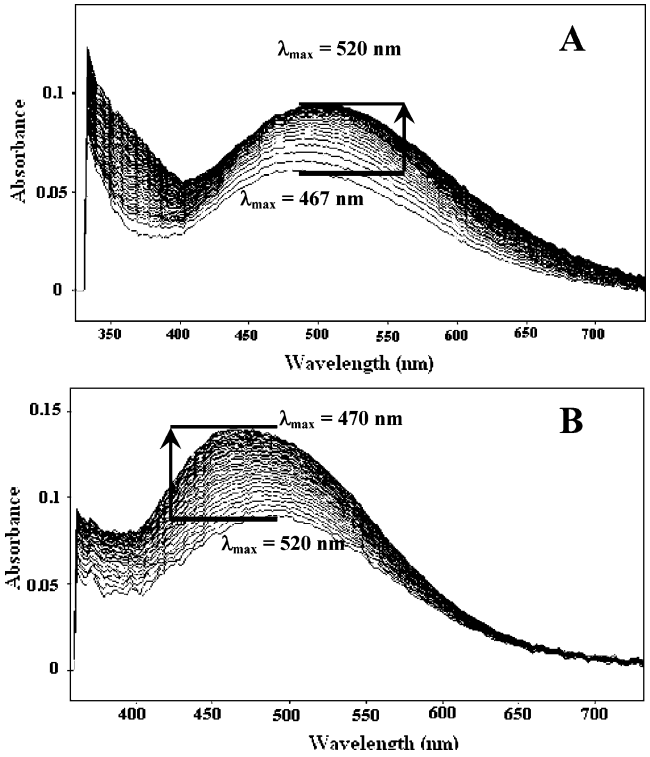


FIGURE 7: A representative spectral change for the reaction between $Fe^{3+}$FbpA-NTA and Tiron under pseudo-first-order conditions (Tiron in excess). (A) Initially, the $\lambda_{max}$ corresponding to the LMCT band of $Fe^{3+}$FbpA-NTA undergoes a red shift (from 467 to 520 nm) in stage I. (B) In stage II this new intermediate absorbance maximum shifts to 470 nm, corresponding to the characteristic LMCT band of the $Fe(Tiron)_3^{9-}$ complex. Conditions for (A) and (B): [$Fe^{3+}$FbpA-NTA] = $1.02 \times 10^{-4}$ M, [Tiron] = $2.5 \times 10^{-3}$ M, pH 6.5, 0.05 M MES, 0.1 M $NaClO_4$, 25 °C.

show a dependency on Tiron concentration. The larger of the two apparent rate constants ($k^{I}_{obs}$), corresponding to stage I, is linearly dependent on Tiron concentration (Figure 9A), while the smaller apparent rate constant ($k^{II}_{obs}$), corresponding to stage II, shows saturation at high Tiron concentration (Figure 9B). These dependencies on the chelate concentration are different from that seen for the reaction of $Fe^{3+}$FbpA-$PO_4$ with EDTA: stage I for EDTA shows a saturation profile while stage II shows a linear dependency.

*(A) Stage I for $Fe^{3+}$FbpA-$PO_4$ + Tiron.* The stage I rate constant ($k^{I}_{obs}$) is linearly dependent on the Tiron concentration (Figure 9A) and is attributed to a direct attack of Tiron on $Fe^{3+}$FbpA-$PO_4$ (eq 14). A linear fit of the rate law (eq

$$Fe^{3+}\text{FbpA-PO}_4 + \text{Tiron} \rightarrow Fe^{3+}\text{FbpA(PO}_4\text{)(Tiron)} \quad k_1 \quad (14)$$

$$k^{I}_{obs} = k_1[\text{Tiron}] \quad (15)$$

15) to the data (Figure 9A) yields $k_1 = 1.6 \times 10^1$ $M^{-1}$ $s^{-1}$ from the slope and a zero intercept. At the end of stage I an intermediate $Fe^{3+}$FbpA($PO_4$)(Tiron) is generated, in which Tiron has a direct interaction with $Fe^{3+}$. This is consistent with the observed red shift in the spectral profile resulting from a first coordination shell interaction between Tiron, a catecholate, and $Fe^{3+}$ (*33*). The intermediate generated at the end of stage I, $Fe^{3+}$FbpA($PO_4$)(Tiron), is significantly different from the intermediate generated at the end of stage I in the reaction between $Fe^{3+}$FbpA-$PO_4$ and EDTA, $Fe^{3+}$-FbpA-EDTA.

*(B) Stage II for $Fe^{3+}$FbpA-$PO_4$ + Tiron.* The smaller rate constant ($k^{II}_{obs}$) for stage II shows a saturation profile at high Tiron concentrations (Figure 9B), which is attributed to two successive reactions involving one Tiron molecule and the intermediate species generated at the end of stage I, $Fe^{3+}$-FbpA($PO_4$)(Tiron), as shown in eqs 16 and 17. A rate law assuming reaction 16 is a rapid preequilibrium is given by eq 18. A nonlinear fit of eq 18 to the data (Figure 9B) yields

$$Fe^{3+}\text{FbpA(PO}_4\text{)(Tiron)} + \text{Tiron} \rightleftharpoons Fe^{3+}\text{FbpA(PO}_4\text{)(Tiron)}\cdots\text{Tiron} \quad Q_2 \quad (16)$$

$$Fe^{3+}\text{FbpA(PO}_4\text{)(Tiron)}\cdots\text{Tiron} \rightarrow \text{apo-FbpA-PO}_4 + \text{Fe-Tiron} \quad k_3 \quad (17)$$

$$k^{II}_{obs} = \frac{k_3[\text{Tiron}]}{(1/Q_2) + [\text{Tiron}]} \quad (18)$$

$Q_2 = 1.9 \times 10^2$ $M^{-1}$ and $k_3 = 2.8 \times 10^{-2}$ $s^{-1}$.

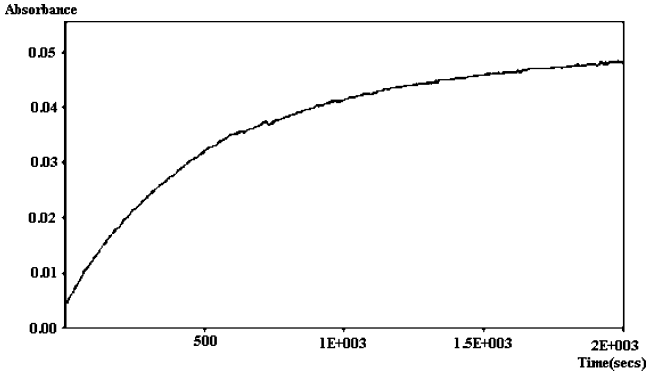


FIGURE 8: A representative absorbance increase at 470 nm for the reaction between $Fe^{3+}$FbpA-$PO_4$ and Tiron under pseudo-first-order conditions (Tiron in excess). Conditions: [$Fe^{3+}$FbpA-$PO_4$] = $9.26 \times 10^{-5}$ M, [Tiron] = $2.5 \times 10^{-3}$ M, pH 6.5, 0.05 M MES, 0.1 M $NaClO_4$, 25 °C.

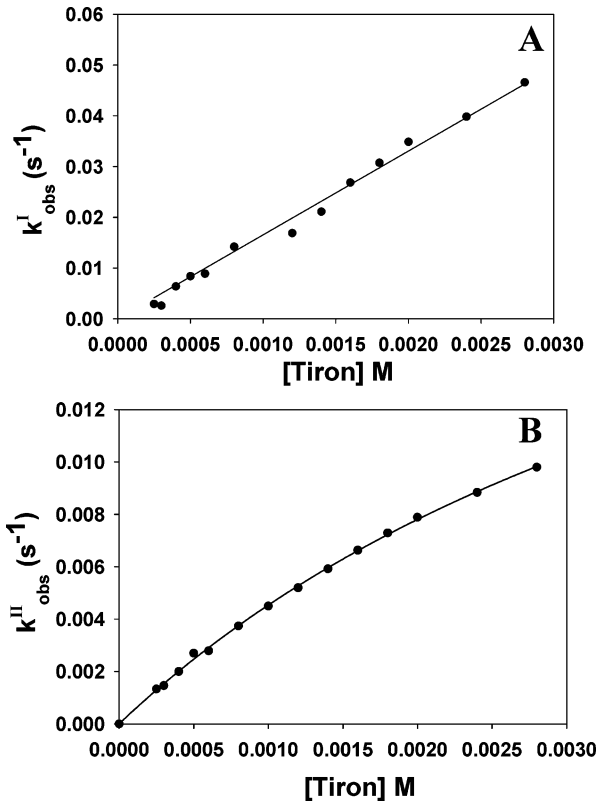


FIGURE 9: (A) Plot of the observed rate constants, $k^I_{obs}$, for stage I as a function of Tiron concentration for the reaction between $Fe^{3+}$-FbpA-$PO_4$ and Tiron. The solid line represents a fit of eq 15 to the data. (B) Plot of the observed rate constants $k^{II}_{obs}$ for stage II for the reaction between $Fe^{3+}$FbpA-$PO_4$ and Tiron. The solid line represents the nonlinear fit of eq 18 to the data. Conditions for (A) and (B): [$Fe^{3+}$FbpA-$PO_4$] = $9.26 \times 10^{-5}$ M, pH 6.5, 0.05 M MES, 0.1 M $NaClO_4$, 25 °C.

*$Fe^{3+}$FbpA-NTA + Tiron.* The reaction between $Fe^{3+}$FbpA-NTA and Tiron shows two distinct single exponential rises in absorbance at $\lambda_{max}$ = 470 nm described by eq 2, which correspond to stage I and stage II (Figure 10). The observed rate constants for both processes show a dependency on Tiron concentration. The faster process, corresponding to stage I ($k^I_{obs}$), is linearly dependent on Tiron concentration (Figure 11A), while the slower apparent rate constant ($k^{II}_{obs}$), corresponding to stage II, shows saturation at high Tiron

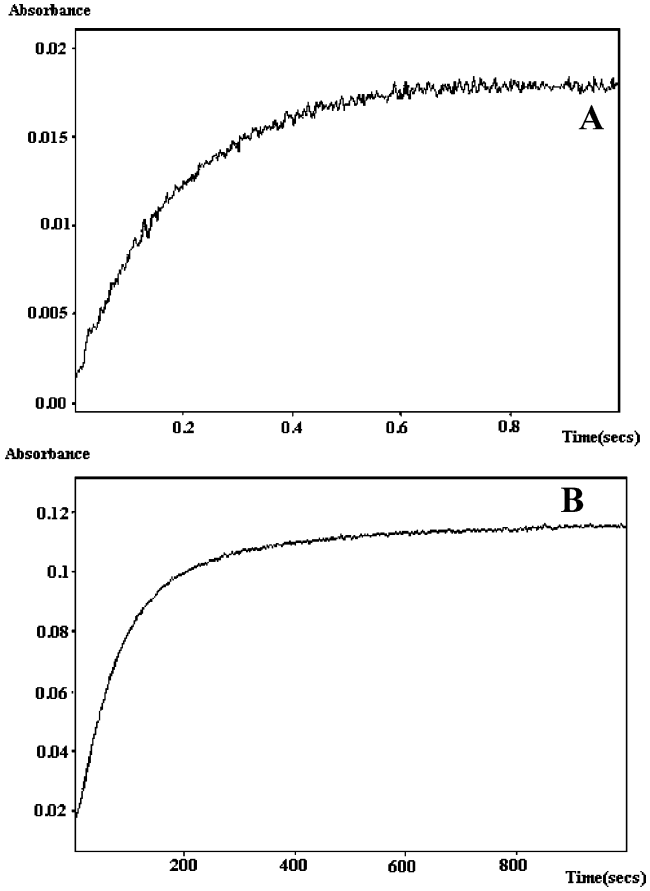


FIGURE 10: A representative absorbance increase at 470 nm for the reaction between $Fe^{3+}$FbpA-NTA and Tiron under pseudo-first-order conditions (Tiron in excess). (A) Stage I. (B) Stage II. Conditions for (A) and (B): [$Fe^{3+}$FbpA-NTA] = $9.26 \times 10^{-5}$ M, [Tiron] = $1.0 \times 10^{-3}$ M, pH 6.5, 0.05 M MES, 0.1 M $NaClO_4$, 25 °C.

concentration (Figure 11B). The $k_{obs}$ profiles are equivalent to those observed for the $Fe^{3+}$FbpA-$PO_4$ and Tiron system.

*(A) Stage I for $Fe^{3+}$FbpA-NTA + Tiron.* A proposed mechanism for stage I attributed to a direct attack of Tiron on $Fe^{3+}$FbpA-NTA and the rate law are shown in eqs 19 and 20. A fit of eq 20 to the data (Figure 11A) yields $k_1$ =

$$Fe^{3+}\text{FbpA-NTA} + \text{Tiron} \rightarrow Fe^{3+}\text{FbpA(NTA)(Tiron)} \quad k_1 \quad (19)$$

$$k^I_{obs} = k_1[\text{Tiron}] \quad (20)$$

$1.7 \times 10^4$ $M^{-1}$ $s^{-1}$ from the slope and a zero intercept. At the end of stage I an intermediate $Fe^{3+}$FbpA(NTA)(Tiron) is generated with $\lambda_{max}$ = 520 nm, in which Tiron has a direct interaction with $Fe^{3+}$ in $Fe^{3+}$FbpA-NTA. This is consistent with the observed red shift in the spectral profile, and it is almost identical to that seen for the $Fe^{3+}$FbpA-$PO_4$ system.

*(B) Stage II for $Fe^{3+}$FbpA-NTA + Tiron.* The observed rate constant for stage II ($k^{II}_{obs}$) shows a saturation profile at high Tiron concentrations (Figure 11B). This behavior is attributed to two successive reactions involving one Tiron molecule and the intermediate species generated at the end of stage I, $Fe^{3+}$FbpA(NTA)(Tiron), as shown in eqs 21 and 22. Assuming eq 21 is a rapid preequilibrium, the rate law

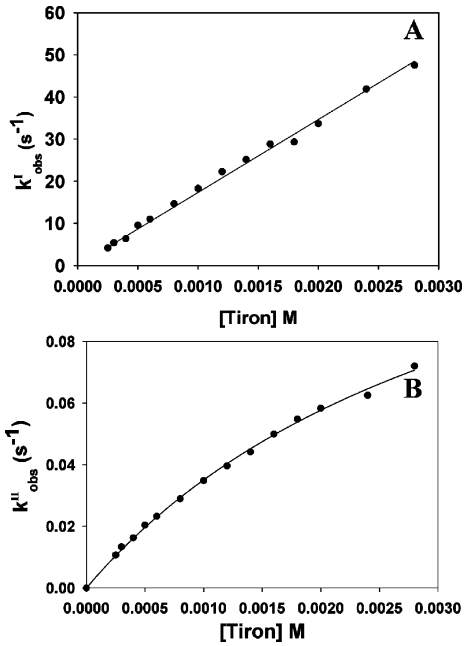


FIGURE 11: (A) Plot of the observed rate constants for stage I for the reaction between $Fe^{3+}$FbpA-NTA and Tiron as a function of Tiron concentration. The solid line represents a fit of eq 20 to the data. (B) Plot of the observed rate constants for stage II for the reaction between $Fe^{3+}$FbpA-NTA and Tiron as a function of Tiron concentration. The solid line represents the nonlinear fit of eq 23 to the data. Conditions for (A) and (B): [$Fe^{3+}$FbpA-NTA] = $9.26 \times 10^{-5}$ M, pH 6.5, 0.05 M MES, 0.1 M $NaClO_4$, 25 °C.

in eq 23 may be derived. A nonlinear fit of eq 23 to the data

$$Fe^{3+}FbpA(NTA)(Tiron) + Tiron \rightleftharpoons Fe^{3+}FbpA(NTA)(Tiron)\cdots Tiron \quad Q_2 \quad (21)$$

$$Fe^{3+}FbpA(NTA)(Tiron)\cdots Tiron \rightarrow apo\text{-}FbpA\text{-}NTA + Fe\text{-}Tiron \quad k_3 \quad (22)$$

$$k^{II}_{obs} = \frac{k_3[Tiron]}{(1/Q_2) + [Tiron]} \quad (23)$$

(Figure 11B) yields $Q_2 = 2.8 \times 10^2$ $M^{-1}$ and $k_3 = 1.6 \times 10^{-1}$ $s^{-1}$. The overall reaction profiles for both $Fe^{3+}$FbpA-$PO_4$ and $Fe^{3+}$FbpA-NTA with Tiron look similar; however, the microscopic constants determined for the two sets of reactions are significantly different.

## DISCUSSION

Table 1 summarizes the microscopic rate constants obtained for the $Fe^{3+}$-exchange reaction (eq 1) on changing the leaving group (synergistic anion X) and entering group (competing chelator L). These data demonstrate that there is a pronounced entering group effect resulting in a change in the reactivity and number of detectable steps in the $Fe^{3+}$ release process upon changing the competing chelator from EDTA to Tiron. There is an increased rate of displacement of NTA over $PO_4^{3-}$ from $Fe^{3+}$FbpA-X with the Tiron competing chelator, and this difference disappears when EDTA is the competing chelator in reaction 1.

*$Fe^{3+}$FbpA-X + EDTA.* Scheme 2 summarizes the reaction paths and microscopic rate constants for the reaction of $Fe^{3+}$-FbpA-X and EDTA. For the most part $Fe^{3+}$FbpA-$PO_4$ and $Fe^{3+}$FbpA-NTA react similarly with EDTA. A common quasi-equilibrium intermediate is formed at the end of stage I which is assumed to have the structure shown in Scheme 2, where EDTA assumes a synergistic anion role, based on spectral data ($\lambda_{max}$ = 460 nm, in close proximity to $\lambda_{max}$ = 467 nm for $Fe^{3+}$FbpA-NTA where the structurally similar NTA acts as a synergistic anion). This is consistent with a recent crystal structure of a FbpA mutant that shows EDTA is capable to acting as a synergistic anion (*30*, *31*).

Stage II for both $Fe^{3+}$FbpA-$PO_4$ and $Fe^{3+}$FbpA-NTA involves the displacement of $Fe^{3+}$ from the common intermediate $Fe^{3+}$FbpA-EDTA by a second EDTA molecule. Figure 12 shows the $Fe^{3+}$ binding pocket and ribbon diagram for $Fe^{3+}$FbpA-$PO_4$ and $Fe^{3+}$*mut*FbpA-EDTA adapted from their respective crystal structures. This comparative analysis indicates that in both structures the anion is acting as a synergistic anion; however, the $Fe^{3+}$ binding pocket in $Fe^{3+}$-FbpA-$PO_4$ appears much less solvent exposed compared to the $Fe^{3+}$ binding pocket in $Fe^{3+}$*mut*FbpA-EDTA. The formation of $Fe^{3+}$FbpA-EDTA as an intermediate at the end of stage I would generate a FbpA complex with an exposed $Fe^{3+}$ center susceptible to attack by another EDTA molecule. We apply these solid-state structural arguments to our mechanistic study with some caution as the two crystal structures were obtained from different yet highly homologous forms of protein, wild-type FbpA from *N. gonorrheae* and a H9Q mutant from *Haemophilus influenzae*. A common intermediate for the product of stage I implies noninvolvement of the leaving group $PO_4^{3-}$ or $NTA^{3-}$ in the species, which is supported by the equivalent values obtained for the microscopic rate constants in stage II for both FeFbpA-$PO_4$ and $Fe^{3+}$FbpA-NTA (Scheme 2; Table 1), and a common $\lambda_{max}$ value (460 nm) for the intermediate reactant (*34*).

The microscopic constants $Q_1$, $k_2$, and $k_3$ for EDTA reaction with $Fe^{3+}$FbpA-$PO_4$ and $Fe^{3+}$FbpA-NTA are equivalent (Scheme 2; Table 1), suggesting a similar mechanistic pathway in both cases. The $Fe^{3+}$FbpA-X$\cdots$EDTA species formed in a rapid preequilibrium in each case involves nonspecific EDTA association with the protein in the second coordination shell of $Fe^{3+}$.

$Fe^{3+}$FbpA-NTA also exhibits a parallel path in stage I involving direct attack by EDTA that is not observed for $Fe^{3+}$FbpA-$PO_4$. Since NTA is larger than $PO_4^{3-}$, it is reasonable to suggest a slight opening of the $Fe^{3+}$ binding cleft similar to that seen in the $Fe^{3+}$*mut*FbpA-EDTA crystal structure (Figure 12) (*30*, *31*), thus allowing direct attack by a competing chelator on the $Fe^{3+}$ center. Weaker $Fe^{3+}$ binding and a more positive $Fe^{3+}/Fe^{2+}$ redox potential for $Fe^{3+}$FbpA-NTA relative to FeFbpA-$PO_4$ (*4*) also suggest a more solvent-exposed $Fe^{3+}$ site in $Fe^{3+}$FbpA-NTA, making the $Fe^{3+}$ more susceptible to direct attack by a competing chelator.

*$Fe^{3+}$FbpA-X + Tiron.* Scheme 3 summarizes the reaction paths and microscopic rate constants for the reaction of $Fe^{3+}$-FbpA-X and Tiron. Both $Fe^{3+}$FbpA-$PO_4$ and $Fe^{3+}$FbpA-NTA react with Tiron via similar pathways but with different macroscopic and microscopic rate constants (Scheme 3; Table 1). The observed rate constants for $Fe^{3+}$FbpA-NTA are larger, indicating a more labile system. This is consistent with thermodynamic data for $Fe^{3+}$FbpA-$PO_4$ and $Fe^{3+}$FbpA-NTA, which show that FbpA affinity for $Fe^{3+}$ is greater when $PO_4^{3-}$ is the synergistic anion and that the FeFbpA-$PO_4$ +

Table 1: Kinetic and Thermodynamic Parameters for Ligand-Exchange Kinetics between $Fe^{3+}$FbpA-X and Competing Chelators, EDTA and Tiron[a]

| protein | chelator | reaction, eq no. | parameters[b] | values | comment |
|---|---|---|---|---|---|
| $Fe^{3+}$FbpA-$PO_4$ | EDTA | 3, 5 | $Q_1$ ($M^{-1}$) | $14.3(0.5) \times 10^1$ | *c* |
| $Fe^{3+}$FbpA-$PO_4$ | EDTA | 4, 5 | $k_2$ ($s^{-1}$) | $2.8(0.3) \times 10^{-1}$ | *c* |
| $Fe^{3+}$FbpA-$PO_4$ | EDTA | 6, 7 | $k_3$ ($M^{-1}\,s^{-1}$) | $5.7(0.2) \times 10^{-3}$ | *d* |
| $Fe^{3+}$FbpA-$PO_4$ | EDTA | 6, 7 | $k_{-3}$ ($s^{-1}$) | $2.3(0.4) \times 10^{-5}$ | *d* |
| $Fe^{3+}$FbpA-NTA | EDTA | 9, 11 | $Q_1$ ($M^{-1}$) | $9.8(0.2) \times 10^1$ | *c* |
| $Fe^{3+}$FbpA-NTA | EDTA | 10, 11 | $k_2$ ($s^{-1}$) | $6.2(0.6) \times 10^{-1}$ | *c* |
| $Fe^{3+}$FbpA-NTA | EDTA | 12, 13 | $k'_1$ ($M^{-1}\,s^{-1}$) | 2.3(0.4) | *c* |
| $Fe^{3+}$FbpA-NTA | EDTA | 12, 13 | $k'_{-1}$ ($s^{-1}$) | $1.3(0.5) \times 10^{-3}$ | *c* |
| $Fe^{3+}$FbpA-NTA | EDTA | 6, 7 | $k_3$ ($M^{-1}\,s^{-1}$) | $1.1(0.1) \times 10^{-3}$ | *d* |
| $Fe^{3+}$FbpA-NTA | EDTA | 6, 7 | $k_{-3}$ ($s^{-1}$) | $4.2(0.2) \times 10^{-5}$ | *d* |
| $Fe^{3+}$FbpA-$PO_4$ | Tiron | 14, 15 | $k_1$ ($M^{-1}\,s^{-1}$) | $1.6(0.4) \times 10^1$ | *c* |
| $Fe^{3+}$FbpA-$PO_4$ | Tiron | 16, 18 | $Q_2$ ($M^{-1}$) | $1.9(0.3) \times 10^2$ | *c* |
| $Fe^{3+}$FbpA-$PO_4$ | Tiron | 17, 18 | $k_3$ ($s^{-1}$) | $2.8(0.1) \times 10^{-2}$ | *c* |
| $Fe^{3+}$FbpA-NTA | Tiron | 19, 20 | $k_1$ ($M^{-1}\,s^{-1}$) | $1.7(0.1) \times 10^4$ | *c* |
| $Fe^{3+}$FbpA-NTA | Tiron | 21, 23 | $Q_2$ ($M^{-1}$) | $2.8(0.2) \times 10^2$ | *c* |
| $Fe^{3+}$FbpA-NTA | Tiron | 22, 23 | $k_3$ ($s^{-1}$) | $1.6(0.1) \times 10^{-1}$ | *c* |

[a] Conditions: pH 6.5, 0.05 M MES, 0.1 M $NaClO_4$, 25 °C. [b] Parameters defined as in the equations listed in column 3 and in Scheme 2 or 3. [c] Stopped-flow kinetic data. [d] Rapid-mixing kinetic data.

Scheme 2: Stepwise Mechanisms for Reaction between $Fe^{3+}$FbpA-$PO_4$ and EDTA, and $Fe^{3+}$FbpA-NTA and EDTA, along with Experimentally Obtained Microscopic Constants

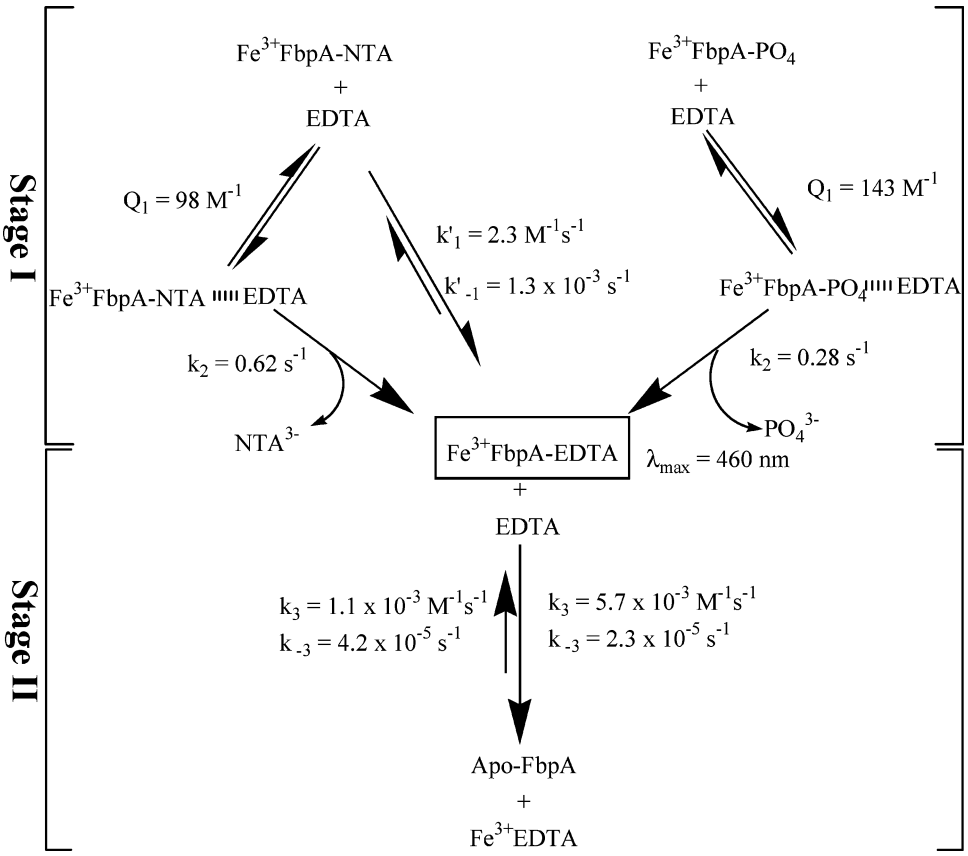


NTA anion-exchange reaction favors FeFbpA-$PO_4$ (*4*, *7*). Additionally, this pronounced NTA lability is consistent with a more exposed $Fe^{3+}$ center in the $Fe^{3+}$FbpA-NTA complex as discussed above. The mechanistic details presented in Scheme 3 indicate a direct attack by Tiron on $Fe^{3+}$ in $Fe^{3+}$-FbpA-X. As expected, the major influence of the synergistic anion leaving group is felt in stage I (cf. $k_1$ values in Scheme 3). The preequilibrium first step in stage II involving attack of a second Tiron chelator does not involve displacement of the synergistic anion, as $Q_2$ is essentially the same for $Fe^{3+}$-FbpA-$PO_4$ and $Fe^{3+}$FbpA-NTA. Here a second Tiron molecule forms a second-coordination shell complex and reacts with the intermediate. Lastly, the final step of $Fe^{3+}$ removal has different rates for the $Fe^{3+}$FbpA-$PO_4$ and $Fe^{3+}$FbpA-NTA systems, suggesting a possible involvement of the synergistic anion in the final release process.

*Kinetics and the Synergistic Anion.* A significant difference in the EDTA and Tiron competition reactions is that EDTA also acts as a synergistic anion and Tiron does not. For the Tiron reactions, the Tiron directly attacks the protein without completely displacing the synergistic anion prior to the attack of a second Tiron; however, the energetics of these processes

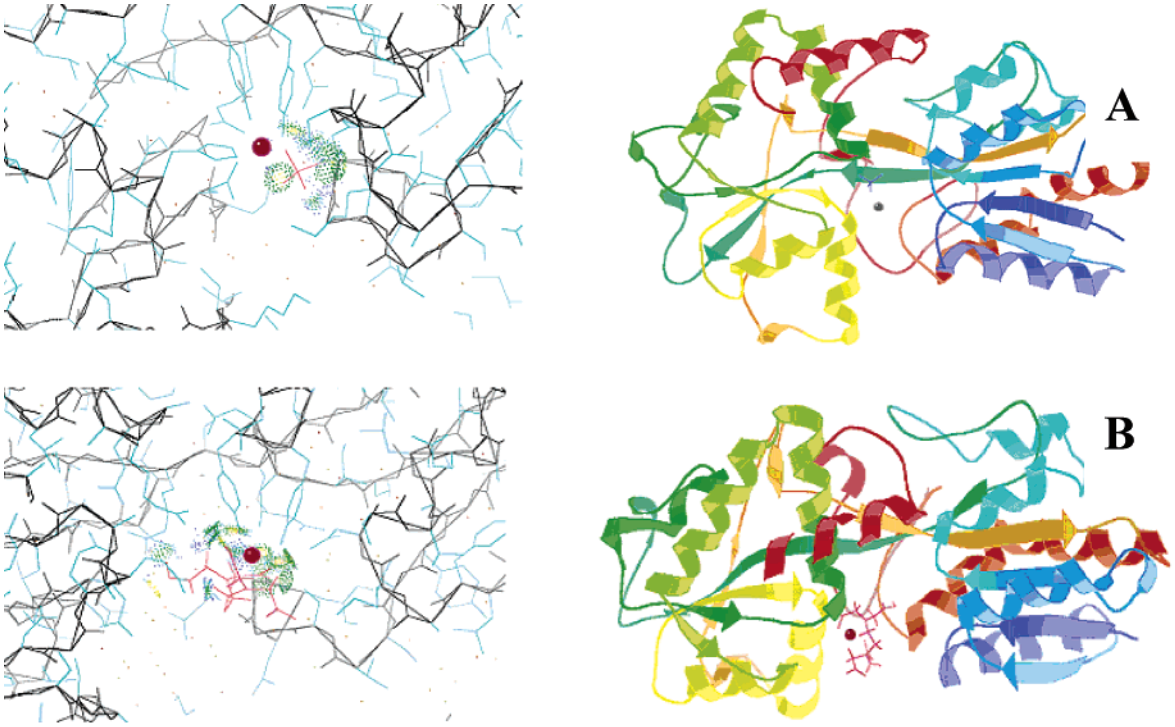


FIGURE 12: $Fe^{3+}$ binding pocket and ribbon diagram for (A) $Fe^{3+}$FbpA-$PO_4$ (PDB ID 1MRPH) and (B) $Fe^{3+}$*mut*FbpA-EDTA (PDB ID 1NNFH). $Fe^{3+}$ binding pocket and ribbon diagram for $Fe^{3+}$FbpA-$PO_4$ and $Fe^{3+}$*mut*FbpA-EDTA generated using crystallographic data from refs *5* and *30*, respectively.

Scheme 3: Stepwise Mechanisms for Reaction between $Fe^{3+}$FbpA-$PO_4$ and Tiron, and $Fe^{3+}$FbpA-NTA and Tiron, along with Experimentally Obtained Microscopic Constants

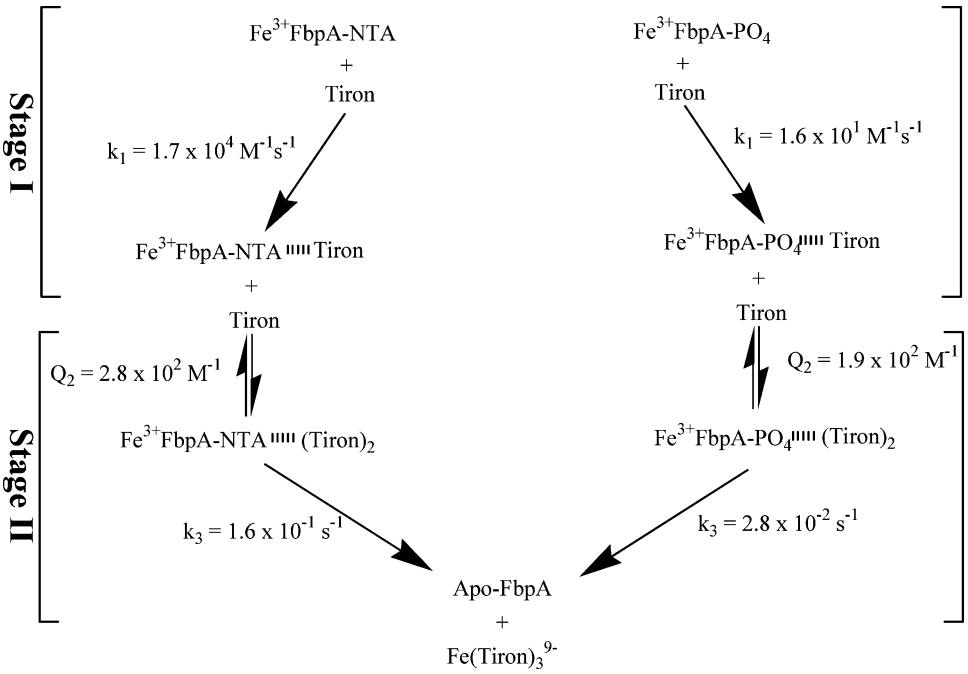


are controlled by the identity of the synergistic anion (Scheme 3). In the mechanism for the EDTA competition, the EDTA acts as a synergistic anion in the process of removing $Fe^{3+}$ from FbpA (Scheme 2). Once the intermediate $Fe^{3+}$FbpA-EDTA is formed, EDTA then becomes the new synergistic anion and the leaving group.

The $Fe^{3+}$ release process from FbpA is strongly modulated by the nature of the synergistic anion present at the first coordination shell of $Fe^{3+}$. The synergistic anion appears to act as the gatekeeper for $Fe^{3+}$ release in both the EDTA and Tiron competition reactions. The larger NTA anion may prevent complete closure of the C and N domains around the $Fe^{3+}$ binding cleft, leaving the $Fe^{3+}$ more exposed and thus enabling a more facile direct attack by Tiron and EDTA. This may also be related to the lower $Fe^{3+}$ binding affinity of the protein in the presence of NTA (*4*).

*Comparison of Chelator Competition and Proton-Driven $Fe^{3+}$ Release.* The important role of the synergistic anion during the $Fe^{3+}$ release process is also supported by the proton-driven dissociation of $Fe^{3+}$ from FbpA, where pro-

tonation of the synergistic anion was found to be the initial step, followed by dissociation of the synergistic anion to form the quasi-intermediate species $Fe^{3+}FbpA(OH_2)_2$ (*25*). Therefore, a synergistic anion in the $Fe^{3+}$FbpA-X complex may also be considered as a "gatekeeper" that controls $Fe^{3+}$ release, whether this process is via a chelator competition reaction or a proton-driven dissociation.

It is of interest to compare our results for Tiron- and EDTA-driven $Fe^{3+}$ dissociation from $Fe^{3+}$FbpA-$PO_4$ with those of our previous study of the $H^+$-driven dissociation of $Fe^{3+}$ from the same protein (*25*). Extrapolation of our data for $H^+$-driven dissociation of $Fe^{3+}$ from micromolar $Fe^{3+}$-FbpA-$PO_4$ to pH 6.5 (*25*) yields the same overall rate as the corresponding reaction in the presence of micromolar EDTA. The difference of course is that EDTA provides a thermodynamic driving force for the reaction and prevents precipitation of $Fe^{3+}_{aq}$ at higher pH. The $Fe^{3+}$ dissociation rate will also increase linearly as the EDTA concentration increases. The dissociation of $Fe^{3+}$ from micromolar $Fe^{3+}$FbpA-$PO_4$ in the presence of micromolar Tiron at pH 6.5 proceeds at a rate 1000-fold greater than either the EDTA- or $H^+$-driven reaction at comparable conditions. These semiquantitative considerations convey the importance and role(s) of a competing $Fe^{3+}$ binding site in the in vivo release of $Fe^{3+}$ at the cytoplasmic membrane. In this respect, the FbpB membrane permease may contain such a competing $Fe^{3+}$ binding site and thereby provide the driving force for release of $Fe^{3+}$ from FbpA.

*FbpA and Mammalian Transferrin.* It is useful to compare aspects of $Fe^{3+}$ release from $Fe^{3+}$FbpA-X driven by a competing chelator as reported here with similar kinetic data for mammalian transferrin. Both bacterial transferrin (FbpA) and mammalian transferrin satisfy an in vivo function to transport $Fe^{3+}$ between membrane receptors. However, there are definitely limits to the validity of this comparison for structural and environmental reasons. First, human transferrin is a bilobal protein in which the two $Fe^{3+}$ binding sites behave somewhat differently with respect to $Fe^{3+}$ release in vivo and in vitro (*8*, *35*). Monolobal FbpA is best compared with N-lobe human transferrin, although the $Fe^{3+}$ ion is more exposed to the external aqueous environment in FbpA (*7*, *36*, *37*). Second, although the residues involved in $Fe^{3+}$ binding are similar, the sequence homology between the two proteins is <20% and the synergistic anions are different, as are their binding sites (*2*). Third, an endosomal pH drop from 7.4 to ~5.6 plays an integral role in the in vivo release of iron from mammalian transferrin, while bacterial transferrin exists in the relatively constant pH 6.5 of the periplasm (*38*). Consequently, our studies reported here were all carried out at pH 6.5.

Both saturation and linear kinetics, as well as dual-mode kinetics, have been observed for chelator-induced $Fe^{3+}$ release from full-length and recombinant N-lobe mammalian transferrin, depending on the competing chelator, as is the case in our study. Kinetic data for mammalian transferrin have been interpreted in terms of a mechanism involving a protein conformational change or breathing mode and displacement of the synergistic carbonate anion. The algebraic form(s) of the rate law is (are) interpreted using a model involving a protein conformational change with parallel displacement of the synergistic anion by the competing chelator. Anion concentration effects on the kinetics of $Fe^{3+}$ release to a chelator have also been interpreted to indicate the presence of anion binding sites on the protein surface. A recent review of the kinetics of chelator-driven $Fe^{3+}$ release from mammalian transferrin has been published (*28*).

While these general observations for the chelator-driven release of $Fe^{3+}$ from mammalian transferrin are in concert with our observations for EDTA- and Tiron-driven release of $Fe^{3+}$ from $Fe^{3+}$FbpA-$PO_4$ and $Fe^{3+}$FbpA-NTA, the details are not. As we report here for FbpA, competing chelators capable of acting as synergistic anions at the $Fe^{3+}$ binding site in transferrin, such as NTA, give rise to a different kinetic profile for competing chelator-driven $Fe^{3+}$ release, compared to competing chelators that are incapable of acting as a synergistic anion. A similar variation on the $Fe^{3+}$ release kinetic profile is also observed for $Fe^{3+}$FbpA-X reacting with EDTA that can act as a synergistic anion and Tiron, which apparently does not act as a synergistic anion. However, a specific comparison of EDTA and Tiron reactions with $Fe^{3+}$-FbpA-X and with Fe-transferrin shows that the kinetic profile and the mechanism of $Fe^{3+}$ release from FbpA and transferrin are different (*39*−*45*).

A major difference between FbpA and transferrin during a chelator competition reaction is the rate of $Fe^{3+}$ release. $Fe^{3+}$ release from FbpA is much faster than that seen for transferrin at comparable conditions (*44*−*46*). The ability of the FbpA to easily exchange its synergistic anion to form a new ternary complex with the competing chelator during the $Fe^{3+}$ release process may contribute to the observed faster rates of $Fe^{3+}$ release from FbpA. The $Fe^{3+}$ in FbpA is also comparatively more exposed to solvent than the $Fe^{3+}$ in transferrin, and this added exposure may also contribute to a more facile exchange. The rate of chelator-facilitated $Fe^{3+}$ release from mammalian transferrin is apparently limited by a "breathing mode", which allows the transferrin to be in an open conformation, thus enabling the attack by a competing chelator at the $Fe^{3+}$ center (*28*, *47*, *48*). This conformational change or so-called breathing mode kinetic dependence appears to be absent in FbpA, and the more solvent-exposed $Fe^{3+}$ center apparently allows a competing chelator to reach the metal center more easily, regardless of the conformation of the protein. Although we have not assigned a breathing mode in $Fe^{3+}$FbpA-X to a specific form of the rate law, certainly a conformational change occurs in the $Fe^{3+}$ release process as noted in our observed spectral shifts and the fact that the crystal structures of the holo and apo form of the protein show an opening of the $Fe^{3+}$ binding site by a 21° rotation around a hinge axis on $Fe^{3+}$ removal (*5*, *6*, *37*). Direct displacement of the synergistic anion in $Fe^{3+}$FbpA-X by EDTA is postulated on the basis of the spectrum of the intermediate, rather than any specific form of the rate law.

## SUMMARY AND CONCLUSIONS

Competing chelators can effectively remove $Fe^{3+}$ from $Fe^{3+}$FbpA-$PO_4$ and $Fe^{3+}$FbpA-NTA, and the kinetics clearly suggest that the competing chelators EDTA and Tiron determine the mechanism and reaction rates. A competing chelator (entering group) that is capable of acting as a synergistic anion, such as EDTA, can form relatively stable intermediates prior to complete $Fe^{3+}$ removal from FbpA. The formation of the intermediate $Fe^{3+}$FbpA-EDTA in reactions with EDTA appears to diminish the kinetic leaving

group effect. However, for a competing chelator such as Tiron, which shows no evidence of acting as a synergistic anion, the exchange kinetics show a significant leaving group effect in that the lability difference between the $Fe^{3+}$FbpA-$PO_4$ and $Fe^{3+}$FbpA-NTA assemblies is pronounced. Regardless of the nature and the relative stabilities of the intermediates formed during chelator-competition reactions, $Fe^{3+}$ release is facilitated by the destabilizing effect of these newly formed ternary complex intermediates. The synergistic anions clearly appear to control the kinetics of the $Fe^{3+}$FbpA-X reactions with Tiron. This ability of the synergistic anion to modulate the kinetics of $Fe^{3+}$ release along with its ability to modulate the thermodynamics of $Fe^{3+}$ release (*4*, *7*) further establishes the synergistic anions as crucial players in periplasmic $Fe^{3+}$ transport in Gram-negative bacteria.

## REFERENCES


1. Crichton, R. R. (2001) *Inorganic biochemistry of iron metabolism: from molecular mechanism to clinical consequences*, 2nd ed., Wiley, New York.
2. Mietzner, T. A., Tencza, S. B., Adhikari, P., Vaughan, K. G., and Nowalk, A. J. (1998) Fe(III) periplasm-to-cytosol transporters of Gram-negative pathogens, *Curr. Top. Microbiol. Immunol. 225*, 114−135.
3. Anderson, D. S., Adhikari, P., Nowalk, A. J., Chen, C. Y., and Mietzner, T. A. (2004) The hFbpABC transporter from *Haemophilus influenzae* functions as a binding-protein-dependent ABC transporter with high specificity and affinity for ferric iron, *J. Bacteriol. 186*, 6220−6229.
4. Dhungana, S., Taboy, C. H., Anderson, D. S., Vaughan, K. G., Aisen, P., Mietzner, T. A., and Crumbliss, A. L. (2003) The influence of the synergistic anion on iron chelation by ferric binding protein, a bacterial transferrin, *Proc. Natl. Acad. Sci. U.S.A. 100*, 3659−3664.
5. Bruns, C. M., Nowalk, A. J., Arvail, A. S., McTigue, M. A., Vaughan, K. G., Mietzner, T. A., and McRee, D. E. (1997) Structure of *Haemophilus influenzae* $Fe^{3+}$-binding protein reveals convergent evolution within a superfamily, *Nat. Struct. Biol. 4*, 919−924.
6. Bruns, C. M., Anderson, D. S., Vaughan, K. G., Williams, P. A., Nowalk, A. J., McRee, D. E., and Mietzner, T. A. (2001) Crystallographic and biochemical analyses of the metal-free *Haemophilus influenzae* $Fe^{3+}$-binding protein, *Biochemistry 40*, 15631−15637.
7. Taboy, C. H., Vaughan, K. G., Mietzner, T. A., Aisen, P., and Crumbliss, A. L. (2001) $Fe^{3+}$ coordination and redox properties of a bacterial transferrin, *J. Biol. Chem. 276*, 2719−2724.
8. Aisen, P. (1998) Transferrin, the transferrin receptor, and the uptake of iron by cells, in *Metal Ions in Biological Systems*, pp 585−631, Dekker, New York.
9. Adhikari, P., Kirby, S. D., Nowalk, A. J., Veraldi, K. L., Schryvers, A. B., and Mietzner, T. A. (1995) Biochemical characterization of a *Haemophilus influenzae* periplasmic iron transport operon, *J. Biol. Chem. 270*, 25142−25149.
10. Anraku, Y. (1968) Transport of sugars and amino acids in bacteria. I. Purification and specificity of the galactose- and leucine-binding proteins, *J. Biol. Chem. 243*, 3116−3122.
11. Barash, H., and Halpern, Y. S. (1975) Purification and properties of glutamate binding protein from the periplasmic space of *Escherichia coli* K12, *Biochim. Biophys. Acta 386*, 168−180.
12. Clark, A. F., Gerken, T. A., and Hogg, R. W. (1982) Proton nuclear magnetic resonance spectroscopy and ligand binding dynamics of the *Escherichia coli* L-arabinose binding protein, *Biochemistry 21*, 2227−2233.
13. Guyer, C. A., Morgan, D. G., and Staros, J. V. (1986) Binding specificity of the periplasmic oligopeptide-binding protein from *Escherichia coli*, *J. Bacteriol. 168*, 775−779.
14. Jacobson, B. L., and Quiocho, F. A. (1988) Sulfate-binding protein dislikes protonated oxyacids. A molecular explanation, *J. Mol. Biol. 204*, 783−787.
15. Medveczky, N., and Rosenberg, H. (1969) Binding and release of phosphate by a protein isolated from *Escherichia coli*, *Biochim. Biophys. Acta 192*, 369−371.
16. Miller, D. M., III, Olson, J. S., Pflugrath, J. W., and Quiocho, F. A. (1983) Rates of ligand binding to periplasmic proteins involved in bacterial transport and chemotaxis, *J. Biol. Chem. 258*, 13665−13672.
17. Schwartz, M., Kellermann, O., Szmelcman, S., and Hazelbauer, G. L. (1976) Further studies on the binding of maltose to the maltose-binding protein of *Escherichia coli*, *Eur. J. Biochem. 71*, 167−170.
18. Smith, M. W., Tyreman, D. R., Payne, G. M., Marshall, N. J., and Payne, J. W. (1999) Substrate specificity of the periplasmic dipeptide-binding protein from *Escherichia coli*: experimental basis for the design of peptide prodrugs, *Microbiology (Reading, U.K.) 145*, 2891−2901.
19. Weiner, J. H., Furlong, C. E., and Heppel, L. A. (1971) Binding protein for L-glutamine and its relation to active transport in *Escherichia coli*, *Arch. Biochem. Biophys. 142*, 715−717.
20. Willis, R. C., and Furlong, C. E. (1974) Purification and properties of a ribose-binding protein from *Escherichia coli*, *J. Biol. Chem. 249*, 6926−6929.
21. Willis, R. C., and Furlong, C. E. (1975) Purification and properties of a periplasmic glutamate-aspartate binding protein from *Escherichia coli* K12 strain W3092, *J. Biol. Chem. 250*, 2574−2580.
22. Dhungana, S., Taboy, C. H., Zak, O., Larvie, M., Crumbliss, A. L., and Aisen, P. (2004) Redox properties of human transferrin bound to its receptor, *Biochemistry 43*, 205−209.
23. Sipe, D. M., and Murphy, R. F. (1991) Binding to cellular receptors results in increased iron release from transferrin at midly acidic pH, *J. Mol. Chem. 266*, 8002−8007.
24. Guo, M., Harvey, I., Yang, W., Coghil, L., Campopiano, D. J., Parkinson, J. A., MacGillivray, R. T., Harris, W. R., and Sadler, P. J. (2003) Synergistic anion and metal binding to the ferric ion-binding protein from *Neisseria gonorrhoeae*, *J. Biol. Chem 278*, 2490−2502.
25. Boukhalfa, H., Anderson, D. S., Mietzner, T. A., and Crumbliss, A. L. (2003) Kinetics and mechanism of iron release from the bacterial ferric binding protein nFbp: Exogenous anion influence and comparison with mammalian transferrin, *J. Biol. Inorg. Chem. 8*, 881−892.
26. Gabricevic, M., Anderson, D. S., Mietzner, T. A., and Crumbliss, A. L. (2004) Kinetics and mechanism of iron(III) complexation by ferric binding protein: The role of phosphate, *Biochemistry 43*, 5811−5819.
27. Dhungana, S., Anderson, D. S., Mietzner, T. A., and Crumbliss, A. L. (2004) Phosphate ester hydrolysis is catalyzed by a bacterial transferrin: Potential implications for in vivo iron transport mechanisms, *J. Inorg. Biochem. 98*, 1975−1977.
28. He, Q.-Y., and Mason, A. B. (2002) Molecular spects of release of iron from transferrin, in *Molecular and Cellular Iron Transport* (Templeton, D. M., Ed.) pp 95−124, Marcel Dekker, New York.
29. Mietzner, T. A., Bolan, G., Schoolnik, G. K., and Morse, S. A. (1987) Purification and characterization of the major iron-regulated protein expressed by pathogenic *Neisseriae*, *J. Exp. Med. 165*, 1041−1057.
30. Shouldice, S. R., Dougan, D. R., Skene, R. J., Tari, L. W., McRee, D. E., Yu, R., and Schryvers, A. B. (2003) High-resolution structure of an alternate form of the ferric ion binding protein from *Haemophilus influenzae*, *J. Biol. Chem. 278*, 11513−11519.
31. Weaver, K. D., and Crumbliss, A. L. (2003) High-resolution structrue of an alternate form of the ferric ion binding protein from *Haemophilus influenzae*, *Chemtracts: Inorg. Chem. 16*, 715−721.
32. Rogers, T. B., Feeney, R. E., and Meares, C. F. (1997) Interaction of anions with iron-transferrin-chelate complexes, *J. Biol. Chem. 252*, 8108−8112.
33. Dhungana, S., Heggemann, S., Heinisch, L., Moellmann, U., Boukhalfa, H., and Crumbliss, A. L. (2001) Fe(III) coordination properties of two new saccharide-based enterobactin analogues: Methyl 2,3,4-tris-O-{N-[2,3-di(hydroxy)benzoyl-glycyl]-aminopropyl}-α-D-glucopyranoside and methyl 2,3,4-tris-O-{N-[2,3-di-(hydroxy)-benzoyl]-aminopropyl}-α-D-glucopyranoside, *Inorg. Chem. 40*, 7079−7086.
34. The final step (stage II) of $Fe^{3+}$ removal has equivalent yet slightly different rate constants for $Fe^{3+}$FbpA-$PO_4$ and $Fe^{3+}$FbpA-NTA, suggesting a similar mechanism with the slight possibility of the synergistic anion's involvement in the final release process. Despite the small differences in $k_3$ values (Scheme 2; Table 1), the rate constants are too close within the experimental error for them to be interpreted as different mechanistic pathways.

35. Aisen, P. (1994) Iron metabolism: an evolutionary perspective, in *Iron metabolism in health and disease* (Brock, J. H., Halliday, J. W., Pippard, M. J., and Powell, L. W., Eds.) pp 1−30, W. B. Saunders, London.
36. MacGillivray, R. T., Moore, S. A., Chen, J., Anderson, B. F., Baker, H., Luo, Y., Bewley, M., Smith, C. A., Murphy, M. E., Wang, Y., Mason, A. B., Woodworth, R. C., Brayer, G. D., and Baker, E. N. (1998) Two high-resolution crystal structures of the recombinant N-lobe of human transferrin reveal a structural change implicated in iron release, *Biochemistry 37*, 7919−7928.
37. McRee, D. E., Bruns, C. M., Williams, P. A., Mietzner, T. A., and Nunn, R. Crystal structure of holo nFbp, PDB ID 1D9Y (to be published).
38. Ferguson, S. J. (1991) Periplasm, in *Prokaryotic structure and function: a new prespective* (Mohan, S., Dow, C., and Coles, J. A., Eds.) pp 311−339, Cambridge University Press, Edinburg, U.K.
39. Nguyen, S. A. K., Craig, A., and Raymond, K. N. (1993) Transferrin: the role of conformational changes in iron removal by chelators, *J. Am. Chem. Soc. 115*, 6758−6764.
40. He, Q.-Y., Mason, A. B., Woodworth, R. C., Tam, B. M., Wadsworth, T., and MacGillivray, R. T. A. (1997) Effect of mutation of aspartic acid 63 on the metal-binding properties of the recombinant N-lobe of human serum transferrin, *Biochemistry 36*, 5522−5528.
41. Bates, G. W., Billups, C., and Saltman, P. (1967) The kinetics and mechanism if iron(III) exchange between chelates and transferrin: The presentation and removal with EDTA, *J. Biol. Chem. 242*, 2816−2821.
42. Baldwin, D. A. (1980) The kinetics of iron release from human transferrin by EDTA. Effects of salts and detergents, *Biochim. Biophys. Acta 623*, 183−198.
43. Baldwin, D. A., and DeSousa, D. M. R. (1981) The effects of salts on the kinetics of iron release from N-terminal and C-terminal monoferric transferrin, *Biochem. Biophys. Res. Commun. 99*, 1101−1107.
44. He, Q.-Y., Mason, A. B., and Woodworth, R. C. (1997) Iron release from recombinant N-lobe and single point Asp63 mutants of human transferrin by EDTA, *Biochem. J. 328*, 439−445.
45. He, Q.-Y., Woodworth, R. C., and Chasteen, N. D. (2003) Anion exchange in human serum transferrin N-lobe: A model study with variant His249Ala, *J. Biol. Inorg. Chem. 8*, 635−643.
46. Kretchmar Nguyen, S. A., Craig, A., and Raymond, K. N. (1993) Transferrin: The role of conformational changes in iron removal by chelators, *J. Am. Chem. Soc. 115*, 6758−6764.
47. Cowart, R. E., Kojima, N., and Bates, G. W. (1982) The exchange of iron(3+) between acetohydroxamic acid and transferrin. Spectrophotometric evidence for a mixed ligand complex, *J. Biol. Chem. 257*, 7560−7565.
48. Cowart, R. E., Swope, S., Loh, T. T., Chasteen, N. D., and Bates, G. W. (1986) The exchange of iron(3+) between pyrophosphate and transferrin. Probing the nature of an intermediate complex with stopped flow kinetics, rapid multimixing, and electron paramagnetic resonance spectroscopy, *J. Biol. Chem. 261*, 4607−4614.

BI0505518